Journal of Catalysis **194,** 211–221 (2000)
doi:10.1006/jcat.2000.2944, available online at http://www.idealibrary.com on IDEAL®

Crystallization Deactivation of Ni–P/SiO_2 Amorphous Catalyst and the Stabilizing Effect of Silica Support on the Ni–P Amorphous Structure

Hexing Li,* Weijiang Wang,† Hui Li,† and Jing-Fa Deng†,[1]

*Department of Chemistry, Shanghai Normal University, Shanghai 200234, People's Republic of China; and †Department of Chemistry, Fudan University, Shanghai 200433, People's Republic of China

Received November 19, 1999; revised April 11, 2000; accepted June 1, 2000

A supported Ni–P amorphous catalyst (Ni–P/SiO_2) was prepared by electroless plating. When the sample was treated at elevated temperatures from 363 to 973 K in N_2 flow for 2.0 h, the XRD patterns and SEM morphologies revealed that the Ni–P amorphous alloy crystallized stepwise from 673 to 873 K. The stabilizing effect of the support on the Ni–P amorphous alloy was observed by DSC, TPO, and TPR, which was attributed to the high dispersion of the Ni–P alloy particles in the support matrix, the affinity of SiO_2 support for the Ni–P alloy particles, and the transfer of the heat produced during the crystallization from the surface to the bulk of the support. The change in the activity of the as-prepared Ni–P/SiO_2 amorphous catalyst during heat treatment was measured using the liquid phase benzaldehyde hydrogenation as a probe and by comparing to that of the corresponding Ni/SiO_2 crystalline catalyst. On one hand, the activity of both two catalysts decreased with the increase of the treating temperature owing to the decrease in surface active Ni atoms caused by the coalescence of small Ni particles at high temperature. On the other hand, the two catalysts exhibited considerably different catalytic behaviors during the heating treatment. (1) Only a smooth decrease in the activity of the Ni/SiO_2 catalyst was observed with the increase of the treating temperature. While an impressive decrease in the activity of the Ni–P/SiO_2 amorphous catalyst was observed in the temperature range from 673 to 873 K corresponding to its crystallization; (2) no significant change in the apparent activation energy (Ea) and the TOF value was observed during the heating pretreatment of the Ni/SiO_2 catalyst. However, a considerable increase in Ea and a decrease in the TOF value were observed after the crystallization of the Ni–P/SiO_2 amorphous catalyst. These results demonstrated a crystallization deactivation of the Ni–P/SiO_2 amorphous catalyst. According to various characterizations, such as EXAFS, XRD, SEM, TEM, XPS, DSC, ICP, TPR, TPO, TPD, and hydrogen chemisorption, the decrease in the number of surface active Ni atoms and the surface P content in the Ni–P alloy, the change in the structural characteristics, and the adsorbing properties of the Ni active sites were the main factors responsible for the deactivation of Ni–P/SiO_2 amorphous catalyst during the crystallization.

[1] To whom correspondence should be addressed. E-mail: jfdeng@srcap.stc.sh.cn.

Key Words: **Ni–P amorphous catalyst; stabilizing effect of the support; crystallization; deactivation; benzaldehyde (BA) hydrogenation.**

INTRODUCTION

Over the past 20 years, amorphous alloys obtained by rapid quenching techniques and chemical reduction with hypophosphite or borohydride have attracted much attention by chemists owing to their superior catalytic activity, selectivity, poison, and corrosion resistance (1–22). Since the amorphous structure is metastable, the crystallization process of the amorphous catalysts could occur spontaneously during the reaction, especially at high temperature. Therefore, studies of the crystallization process and its effect on the catalytic activity of the amorphous catalysts seem essential to supply valuable information for their industrial application. Yamashita *et al.* (23) studied the crystallization process of Ni–B amorphous alloy and found that the amorphous alloy was crystallized step by step. They also found that a La additive in the amorphous alloy could significantly enhance its thermal stability (24). Our previous studies on the Ni–P amorphous alloy film revealed that the diffusion of the alloy component elements was necessary during its crystallization process (25–27). Therefore, inhibition of such a diffusion process by depositing an amorphous alloy on a suitable carrier with high surface area is one of promising routes (28–34) to improve its thermal stability. However, studies of the improvement on the thermal stability of Ni–P amorphous alloy by a suitable support have never been reported so far. In the present work, both the supported and unsupported Ni–P amorphous alloy catalysts were prepared by electroless plating. The crystallization process was investigated by treating the sample at the elevated temperature from 363 to 973 K. The liquid phase benzaldehyde (BA) hydrogenation was employed to examine the effect of the crystallization on the activity of the Ni–P/SiO_2 amorphous catalyst, which revealed a significant

0021-9517/00 $35.00

crystallization deactivation owing to the change in the structural properties of the Ni active sites.

EXPERIMENTAL

Catalyst Preparation

The Ni–P/SiO_2 amorphous catalyst was prepared by the following procedures: 1.0 g SiO_2 (40∼60 meshes, 182 m^2/g) was impregnated with small amount of $NiCl_2$ solution overnight. It was dried at 423 K and further calcined at 623 K for 2.0 h. The Ni^{2+} on the support was then reduced by NaH_2PO_2 in alkaline solution to create crystalline nuclei. After being washed thoroughly with distilled water, the received sample was transferred into 250 ml solution containing $Na_3C_6H_5O_7 \cdot 2H_2O$ (sodium citrate), CH_3COONa, $NiCl_2 \cdot 6H_2O$, and $NaH_2PO_2 \cdot H_2O$ (pH 4∼5) with stirring at 363 K for electroless plating. The reaction lasted about 2.0 h until no significant bubbles were observed in the solution. The resulting Ni–P/SiO_2 amorphous catalyst was washed thoroughly with distilled H_2O until pH 7 was obtained. Then it was further washed with alcohol (EtOH) to remove H_2O, and finally, dried at 363 K in the N_2 atmosphere (denoted as a fresh sample). The resulting catalysts with different Ni loadings were designated as wt% Ni–P/SiO_2 to indicate the weight percentage of Ni on the support. The Ni–P/γ-Al_2O_3 amorphous catalyst was prepared in a similar way by using γ-Al_2O_3 (40∼60 meshes, 190 m^2/g) as a support.

For comparison, a Ni/SiO_2 crystalline catalyst was also prepared in the same procedure as mentioned above by using hydrazine hydrate ($NH_2NH_2 \cdot H_2O$) instead of $NaH_2PO_2 \cdot H_2O$ as a reducing agent.

The heating pretreatment of the samples was carried out in N_2 flow for 2 h. The treating temperature was adjusted from 363 to 973 K.

Catalyst Characterization

The composition and the Ni loading of the as-prepared catalysts were analyzed by ICP. The metal surface area (S_{act}) was determined by hydrogen chemisorption using a dynamic pulse method. The catalyst surface was purged by helium stream (purity of 99.997%, treated with a Chrompack clean-oxygen filter) for 2.0 h at 573 K, which was lower than that reported by Gil *et al.* (35) in order to avoid the crystallization of the amorphous catalysts. After the catalyst was cooled down to 303 K in helium stream, hydrogen pulses were injected until the calculated area of consecutive pulses was constant. Reproducibility of the absorbed hydrogen amount was better than 10%. According to the hydrogenation chemisorption, the S_{act}, the number of surface active Ni atoms and the surface dispersion of the catalyst were calculated assuming H/Ni(s) = 1 and a surface area of 6.5×10^{-20} m^2 per Ni atom, based on an average of the areas for the (100), (110), and (111) planes (36). Hydrogen temperature-programmed desorption (TPD) was carried out in a self-designed apparatus as described previously (37). The system consisted of a sample chamber which was evacuated up to 2.0×10^{-6} torr by a diffusion pump and an analyzing chamber with a vacuum of 1.0×10^{-8} torr. For each of the experiments, hydrogen was preadsorbed at $P_{H_2} = 1.0 \times 10^{-4}$ torr by the catalyst up to saturation at 423 K, which is slightly higher than the present hydrogenation temperature (393 K) since the reaction is exothermic. After the catalyst was cooled down to 303 K in vacuum (2.0×10^{-6} torr), the hydrogen desorption was carried out by raising the temperature from room temperature at a speed of 40 K/min in which the released H_2 was determined by a CFL-203 quadrupole mass spectrometer. Hydrogen adsorption by the silica support could be neglected in the present conditions (38). Amorphous structure and its alteration during the heating pretreatment were determined by X-ray diffraction (XRD, Rigaku Dmax-3C with Cu $K\alpha$ radiation), and extended X-ray absorption fine structure (EXAFS, BL-10B) carried out in the National Laboratory of High Energy Physics (KEK, Tsukuba, Japan). Data were treated by using the EXAFS (II) program (39). The thermal stability was determined by differential scanning calorimetry (DSC, Perkin–Elmer). The surface morphology and the particle size was determined by both the scanning electron micrograph (SEM, JSM-840) and the transmission electron micrograph (TEM, Hitachi H 600). The surface electronic states were determined by the X-ray photoelectron spectroscopy (XPS, Perkin–Elmer PH I 5000C). Surface charging was effectively reduced by using an electron flood gun, as reported by Huchital and Mckeon (40). All binding energy values were calibrated by using the value of contaminant carbon ($C_{1S} = 284.6$ eV) as a reference. Hydrogen temperature programmed reduction (TPR) was carried out in flow of 3% (V/V) H_2/Ar through a catalyst bed with a temperature ramp of 8 K/min. The hydrogen consumption was recorded by a TCD.

Activity Test

The hydrogenation of BA was carried out in the procedure described as follows. In a high-pressure stainless steel autoclave, 1.0 g catalyst was mixed with 40 ml EtOH and 10 ml BA. The pH value of the reaction mixture was adjusted to 4.0 by adding acetic acid. After replacing all the air with H_2 in the reactor, the reactor was heated in an oil bath at the rate of 80 K/h until 393 K. Then was filled with H_2 up to 1.00 MPa. When the pressure reached a steady state, the hydrogenation was started immediately by stirring the reaction mixture vigorously with a magnetic stirrer. The stirring effect was carefully investigated and a stirring rate of 1200 rpm was employed, which was then turned to be sufficient to eliminate the diffusion limit. The initial hydrogenation activity was determined by monitoring the change of

the pressure with the time which was then turned into H_2 uptake rate per gram Ni (R_{H_2} = mmol/h · g Ni) according to the ideal gas equation (29). After reaction for 4 h in which the P_{H_2} remained constant at 1.0 MPa, the products were analyzed by a GC 1102 gas chromatography with a flame ionization detector equipped with a 25-m OV 101 capillary column, and a 353–533 K oven temperature programmed at a ramp of 4 K/min. The reaction conversion and selectivity were determined by the product analysis and the TOF values were calculated according to the hydrogen chemisorption.

RESULTS AND DISCUSSION

Crystallization of the Ni–P Amorphous Alloy and the Change in Structural Properties

Figure 1 shows the change in the XRD patterns of the Ni–P/SiO_2 amorphous catalyst during the heating pretreatment. By subtracting the broad peak around $2\theta = 22^\circ$ from the amorphous SiO_2 (Fig. 1a), only one broad peak around $2\theta = 45^\circ$ was observed for the fresh Ni–P/SiO_2 sample (Fig. 1b) similar to that found in the Ni–P amorphous alloy obtained by rapid quenching techniques (41), indicating that Ni and P on the support existed in an amorphous alloy (42). When the sample was treated at temperatures below 623 K, no significant change in the XRD patterns was observed. However, various crystalline diffractional peaks corresponding to metallic Ni appeared on the XRD patterns when the sample was treated at 673 K. The intensity of these crystallized Ni peaks increased gradually with the increase of treating temperature from 673 to 773 K, as shown in Figs. 1c–1e. No crystallized Ni_3P phase was observed at temperatures <873 K. This was mainly attributed to the low content of Ni_3P phase which was highly dispersed in the silica matrix. Due to the increase of the Ni_3P phase content with the increase of treating temperature and the gathering of the Ni_3P particles at high temperature, finally, the Ni_3P phase was observed on the XRD pattern when the sample was treated at 873 K, as shown in Fig. 1f. By using the unsupported Ni–P amorphous alloy to eliminate the dispersing effect from the support, the XRD patterns clearly demonstrated that the Ni_3P phase really formed simultaneously with the crystallized Ni phase, as shown in Fig. 2. In addition, the gradual formation of the Ni_3P phase could also be observed by using the Ni–P/SiO_2 sample with higher Ni loading (12.2 wt%). Therefore, it could be concluded that the crystallization process of the Ni–P/SiO_2 amorphous catalyst proceeded stepwise during which both the crystallized Ni and Ni_3P phase formed simultaneously. The crystallization process was eventually completed around 873 K, since the XRD patterns remained unchanged when the treating temperature was further increased.

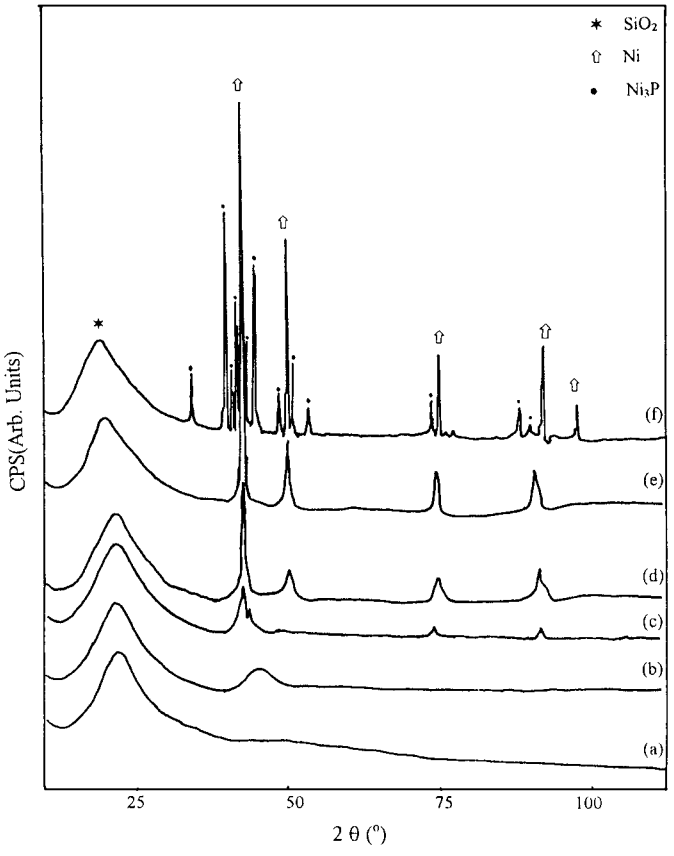

FIG. 1. XRD patterns of (a) SiO_2 and the Ni–P/SiO_2 sample (3.0 wt% Ni) pretreated at temperatures of (b) 363, (c) 673, (d) 723, (e) 773, and (f) 873 K.

The structural transformation of Ni–P/SiO_2 sample during heating pretreatment was further confirmed by EXAFS. Figure 3 shows the radial distribution functions (RDF) obtained from $\chi(k)k^3$ Ni edge by the fast Fourier transformation. As shown in Figs. 3a and 3b, only one broad FT amplitude peak around $R = 1.3\sim2.8$ Å was observed for both the Ni–P/SiO_2 and the unsupported Ni–P samples, indicating that they were present in a typical amorphous structure with no long-range but only short-range ordering structure confined within the first-near-neighbor atom layer (43). After being treated at 873 K, as shown in Fig. 3c, the strength of the original peak increased considerably and two small additional peaks appeared at longer distance ($R = 4\sim5$ Å), indicating the transformation from the amorphous structure to a well ordered crystalline structure during the heating treatment. The similar RDF curve in Fig. 3c and that in Fig. 3d obtained from the Ni foil demonstrated a complete crystallization of Ni–P/SiO_2 sample at 873 K.

Figure 4 shows the change in the SEM morphologies of Ni–P/SiO_2 amorphous catalyst during the heating pretreatment. For the fresh sample, the support was covered by a thin layer of the cotton like clusters of Ni–P amorphous alloy, which was composed of thousands of small particles of

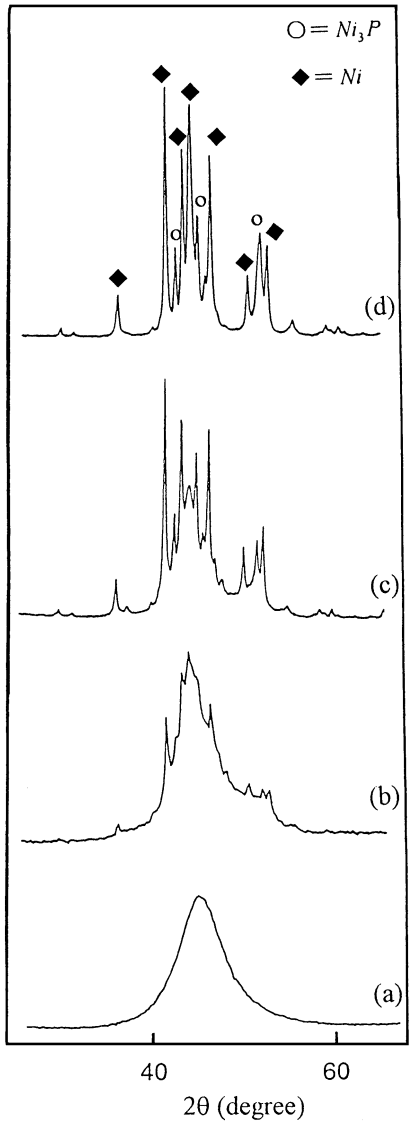

FIG. 2. XRD patterns of unsupported Ni–P amorphous alloy film treated at (a) 570, (b) 580, (c) 590, and (d) 610 K. The unsupported Ni–P amorphous alloy crystallized at lower temperature than the corresponding Ni–P/SiO_2 amorphous catalyst further confirmed the stabilizing effect of the silica support.

Ni–P amorphous alloy. Due to the resolution limit of the available SEM, the TEM was employed instead of SEM to show the shape and size of the Ni–P alloy particles on the SiO_2 support. By using the unsupported Ni–P amorphous catalyst instead of the Ni–P/SiO_2 amorphous catalyst, the TEM morphology clearly revealed that the Ni–P particles were spherical with the average particle size around 100 nm, as shown in Fig. 5. It was reasonable to conclude that the Ni–P alloy particles on the SiO_2 support exhibited similar shape and particle size since both the unsupported and supported Ni–P amorphous catalysts were prepared in the same procedure and under the same conditions. Furthermore, the hydrogen chemisorption also demonstrated that

TABLE 1

Characters of the As-Prepared Catalysts before and after Heating Pretreatment

Catalyst	Composition	Ni loading (wt%)	S_{active} (m^2/g Ni)	Surface active Ni atoms ($\times 10^{19}$)[a]
Fresh Ni–P/SiO_2	$Ni_{86}P_{14}$	3.0	25	1.2
Treated Ni–P/SiO_2[b]	$Ni_{86}P_{14}$	3.0	15	0.69
Fresh Ni/SiO_2	Ni	3.0	32	1.5
Treated Ni/SiO_2[b]	Ni	3.0	17	0.78

[a] Calculated assuming that the average area of one Ni atom is 6.5×10^{-20} m^2.

[b] Treated at 873 K for 2.0 h.

the surface active areas (S_{act}) of both the two catalysts were nearly the same. When the sample was treated from 673 to 873 K, these small Ni–P alloy particles gradually gathered into big lumps and finally, the fine crystalline particles were observed. Consistent with the XRD patterns, it also demonstrated that the crystallization of Ni–P/SiO_2 amorphous catalyst started at 673 K and completed at 873 K since the surface morphology did not change considerably at temperatures higher than 873 K.

Some of the structural characters of the Ni–P/SiO_2 and the corresponding Ni/SiO_2 samples with and without heating pretreatment are summarized in Table 1. One can see

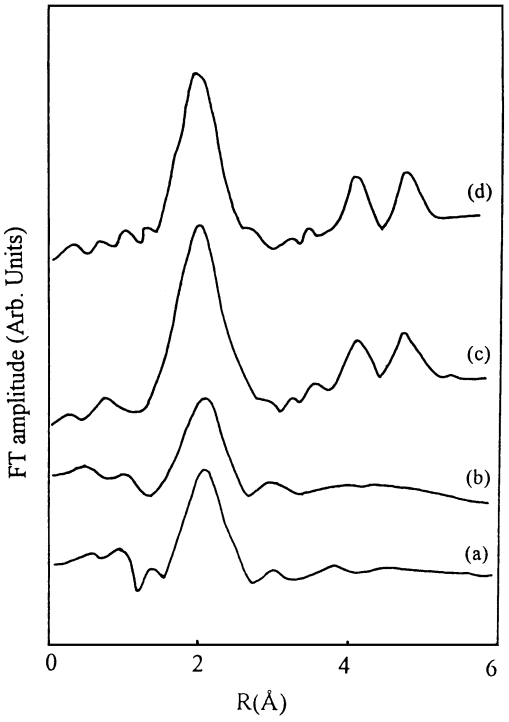

FIG. 3. RDF curves of (a) the fresh Ni–P sample, (b) the fresh Ni–P/SiO_2 sample, (c) the Ni–P/SiO_2 sample being treated at 873 K, and (d) the pure Ni foil.

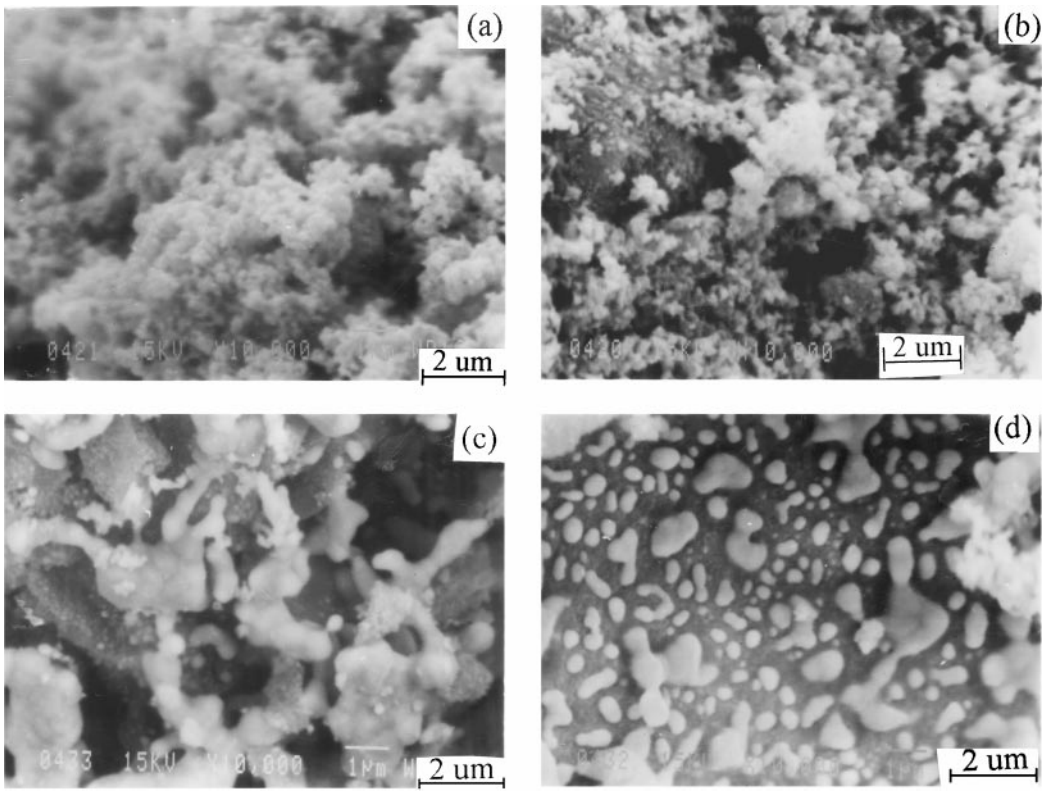

FIG. 4. SEM morphologies of Ni–P/SiO_2 sample (12.2 wt% Ni) pretreated at (a) 363, (b) 673, (c) 773, and (d) 873 K.

that both the S_{act} and the number of surface active Ni atoms decreased greatly after being treated at high temperature, while no significant change in the Ni loading and the composition of Ni–P alloy was observed.

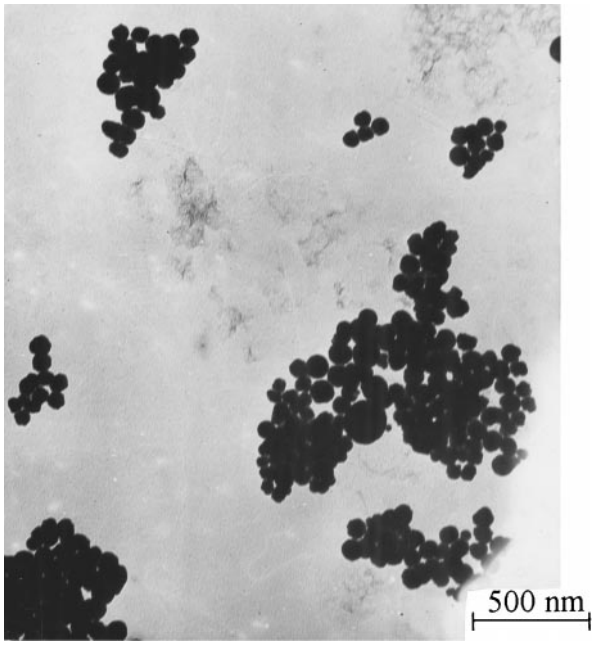

FIG. 5. TEM morphology of unsupported fresh Ni–P sample.

The XPS spectra of the as-prepared catalysts are shown in Fig. 6. In $Ni_2P_{3/2}$ level, one can see that nearly all the nickel species in the as-prepared Ni–P, Ni–P/SiO_2, and Ni/SiO_2 samples are present in the metallic state corresponding to the binding energy (BE) around 853.1 eV. Similarly, as shown in the P_{2P} level, most of the phosphorus species are also present in P^0 state (here, the superscription means the oxidation number of P is equal to 0) corresponding to the BE of 130.0 eV. According to Fig. 6, the following conclusions could be obtained. (1) The electronic interaction between Ni and P in the Ni–P alloy could be neglected since the BE values of Ni and P are exactly the same as those of pure nickel foil and pure red phosphorus, respectively (44). It should be noted that the electron transfer between Ni and P in Ni–P amorphous alloy was inconsistent in the literature. Some reported that the electron transferred from Ni to P (23, 45–47); some reported that there was no electron transfer between Ni and P (48); While others reported that the electron transferred from P to Ni (49–50). Our results revealed that the direction of the electron transfer was strongly dependent on the surface content of P. When P content is very high, Ni donates electrons to P; when P content is very low, Ni accepts electrons from Ni; when P content is about 25 atom% (i.e., Ni_3P), no significant electron transfer between Ni and P could be observed. These results were supported by the calculation of the charge density on Ni and P atoms in Ni_MP amorphous alloy with the DFT

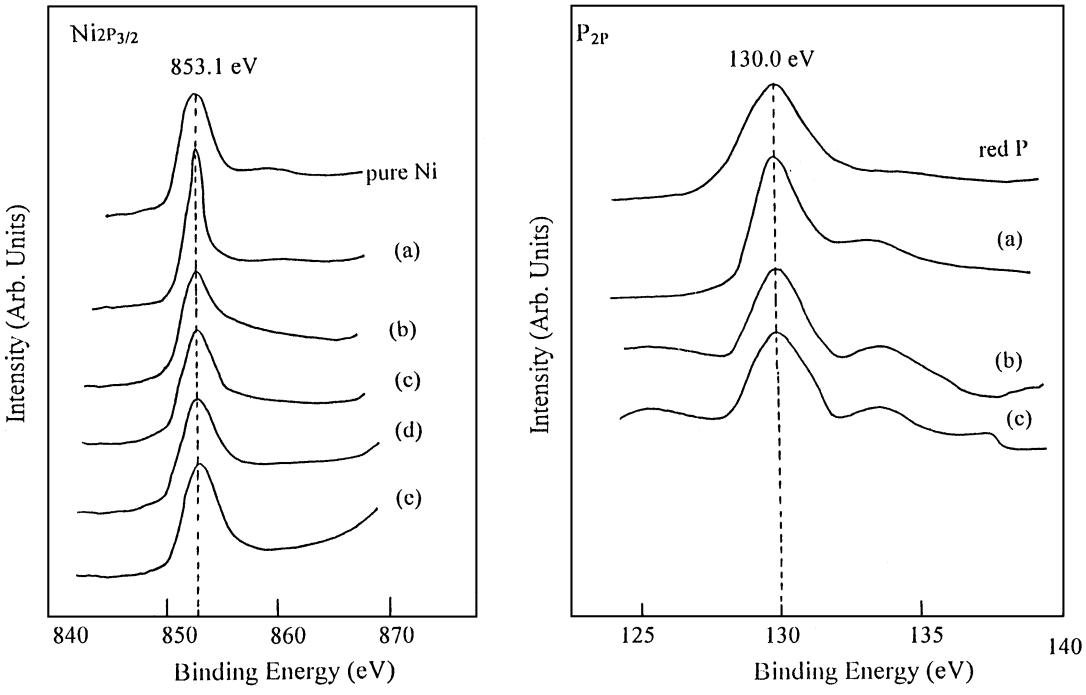

FIG. 6. XPS spectra of $Ni_{2P3/2}$ and P_{2P} of the pure Ni foil, pure red P, and (a) the fresh Ni–P amorphous alloy, (b) the fresh Ni–P/SiO_2 (3.0 wt% Ni) sample, (c) the Ni–P/SiO_2 sample being treated at 873 K, (d) the fresh NiP/SiO_2 (3.0 wt% Ni) sample, and (e) the Ni/SiO_2 sample being treated at 873 K.

method (Table 2), where *M* represents the atom% of Ni in the Ni–P alloy. No significant electron transfer between Ni and P was observed in the present Ni–P/SiO_2 amorphous catalyst since the surface P content was about 27 atom%, which was close to that of Ni_3P. (2) The similar BE values of supported and unsupported Ni–P samples demonstrated that there is no significant electronic interaction between Ni–P alloy and the silica support. (3) After crystallization, no significant BE shift of either Ni or P was observed possibly due to the formation of only Ni_3P alloy (25 atom% P content) on one hand and the lack of electronic interaction between Ni and SiO_2 or P and SiO_2 on the other hand. (4) The surface compositions of the fresh and the crystallized Ni–P/SiO_2 samples were determined as $Ni_{73}P_{27}$ and $Ni_{93}P_7$, respectively. One possible reason for the decrease in surface P content was the sublimation of P at high temperature since the melting point of free P is only about 873 K. However, as reported previously, the P in the Ni–P alloy was very stable (25). According to the ICP analysis, it was also found that no significant change in the bulk composition of Ni–P/SiO_2 sample was observed after being treated at 873 K for 2 h, as shown in Table 1. Therefore, the decrease in the surface P content of Ni–P/SiO_2 sample after crystallization was mainly attributed to the spillover of the P species into the silica matrix at high temperature.

TABLE 2

Charge Distribution on Ni and P Atoms in Ni_MP Amorphous Alloy[a]

Sample	P	Ni[1][b]	Ni[2]	Ni[3]	Ni[4]	Ni[5]	Ni[6]
NiP	−0.1221[c]	0.1221					
Ni_2P	−0.1463	0.0454	0.1009				
Ni_3P[d]	−0.0163	0.0061	0.0051	0.0051			
Ni_6P	0.1518	−0.0153	−0.0303	−0.0303	−0.0153	−0.0303	−0.0303

[a] *M* represents the atom% in the Ni–P amorphous alloy.

[b] The number in [ ] represents the different Ni atoms. For example, there is only one Ni atom in NiP alloy while there are 6 Ni atoms in Ni_6P.

[c] Negative value represents electron-rich and positive value represents electron-deficient.

[d] Although the calculation shows some electron transfer between Ni and P in Ni_3P, however, the value is too small to be detected by XPS.

The Stabilizing Effect of the Support on the Ni–P Amorphous Alloy

Figure 7 shows the DSC curves of Ni–P/SiO_2 amorphous catalyst with different Ni loadings and the unsupported Ni–P amorphous alloy. Besides the endothermic peak around 373 K owing to the loss of the absorbed water from the samples, the exothermic peaks were attributed to the crystallization of the Ni–P amorphous alloy since it was thermodynamically metastable (32). The peak temperature could roughly represent the crystallization temperature (T_c) of the Ni–P amorphous alloy (2). Therefore, the higher T_c of the Ni–P/SiO_2 than that of the Ni–P amorphous alloy demonstrated the stabilizing effect of the support, which could be understood by considering the following factors:

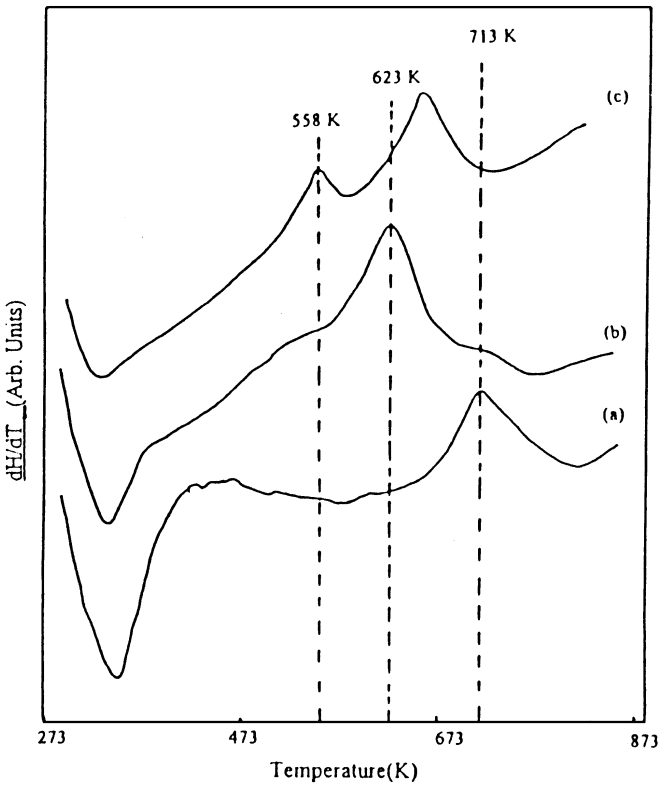

FIG. 7. DSC curves of the Ni–P/SiO_2 amorphous catalysts with Ni loading (wt%) of (a) 3.0, (b) 12.2, and (c) unsupported Ni–P amorphous alloy.

(A). The dispersion of Ni–P amorphous alloy on the support. As shown in Fig. 7 and Table 3, with the increase of Ni loading, both the T_c and the dispersion of the Ni–P/SiO_2 amorphous catalyst decreased, showing the promoting effect of the dispersion on the thermal stability of the Ni–P amorphous alloy. According to our previous study on the crystallization process of Ni–P amorphous alloy film (25), the gathering of small Ni–P alloy particles and the segregation of various crystallites occurred during the crystallization process. Such phenomena were also observed by XRD and SEM during the crystallization of the present Ni–P/SiO_2 amorphous catalyst, as shown in Figs. 1 and 4, respectively. This implied that the diffusion of the component elements in the Ni–P amorphous alloy was essential for the crystallization process of all Ni–P amorphous alloys. Therefore, the promoting effect of the dispersion on the thermal stability of Ni–P amorphous alloy could be attributed to its effective inhibition on the diffusion and gathering processes during the heating treatment.

TABLE 3

Ni Loading, Composition, Dispersion, and the Crystallization Temperature (T_c) of Ni–P Based Amorphous Catalysts

Catalyst	Composition (atom %)	Dispersion (%)	T_c (K)
Ni–P/SiO_2 (3.0 wt% Ni)	$Ni_{86}P_{14}$	4.0	713
Ni–P/SiO_2 (5.2 wt% Ni)	$Ni_{86}P_{14}$	3.0	673
Ni–P/SiO_2 (12.2 wt% Ni)	$Ni_{86}P_{14}$	1.2	623
Ni–P/γ-Al_2O_3 (3.0 wt% Ni)	$Ni_{86}P_{14}$	4.2	745
Unsupported Ni–P	$Ni_{87}P_{13}$	1.0	558

(B). The support function as a heat sink. According to the DSC curves in Fig. 7, the crystallization of Ni–P amorphous alloy is an exothermic process occurred at high temperature. The released heat would raise the temperature resulting in an acceleration of the further crystallization. In the presence of the support, the released heat could be transferred from the surface to the support matrix (41), which inhibited the increase of the surface temperature and in turn, improved the thermal stability of Ni–P amorphous alloy on the support surface.

(C). The interaction between the Ni–P amorphous alloy and the support. Although no significant electronic interaction between Ni–P alloy and silica support was detected by XPS spectra, we still believe that there was a certain kind of interaction between the Ni–P alloy and the silica support based on the following results. (1) As shown in Table 3, the 12.2 wt% Ni–P/SiO_2 amorphous catalyst still exhibited much higher thermal stability than that of the unsupported Ni–P even though their dispersions were nearly the same; (2) As can be seen from the data in Table 3, the Ni–P/Al_2O_3 amorphous catalyst exhibited much higher T_c than that of Ni–P/SiO_2 at the same dispersion. This could be attributed to the stronger interaction between metallic Ni and Al_2O_3 support than of SiO_2, although there was also no electronic interaction between the Ni–P alloy and the Al_2O_3 support according to the XPS characterization; (3) As shown in Fig. 8, the TPO curve revealed that the 12.2 wt% Ni–P/SiO_2 sample could not be oxidized until 573 K. However, the unsupported Ni–P amorphous alloy whose dispersion degree was almost the same as that of the Ni–P/SiO_2 sample could be easily oxidized in the air even at room temperature; (4) In addition, the higher TPR peak temperature of the supported $NiCl_2$ than that of the unsupported $NiCl_2$, as shown in Fig. 9, could also be attributed to the interaction between Ni^{2+} ions and the SiO_2 support. In contrast to the interaction between the Ni–P alloy and the SiO_2 support, the electronic interaction between Ni^{2+} ions and the SiO_2 support was determined by XPS. As a summary, we concluded there was a certain kind of interaction between the Ni–P alloy and the silica support. Possibly, it could be attributed to the affinity of the SiO_2 support for the Ni–P alloy. Such an interaction had no effect on the surface electronic states of Ni and P, but it could prevent the contact of the Ni–P alloy with oxygen and also prevent the gathering of Ni–P alloy particles at high temperature (51–54), which resulted in the higher TPO peak temperature

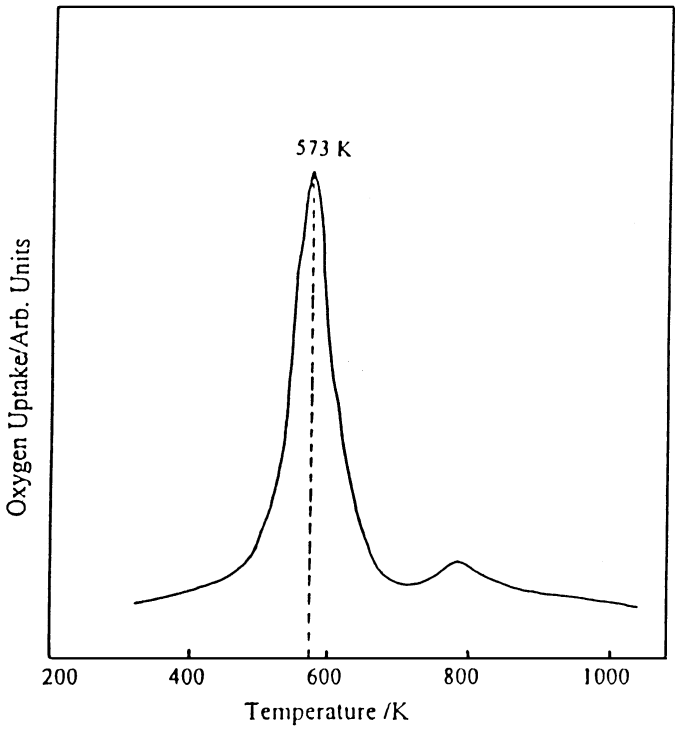

FIG. 8. TPO curve of the fresh Ni–P/SiO_2 amorphous catalyst (12.2 wt% Ni).

and the higher crystallization temperature of the Ni–P/SiO_2 amorphous catalyst. The affinity of the SiO_2 support for the Ni–P alloy was further supported by the fact that only less than 1 ppm Ni species was detected by ICP in the reaction solution after the Ni–P/SiO_2 amorphous catalyst was employed in the hydrogenation for more than 24 h under the present reaction conditions. The leaching away of Ni species in the Ni–P/SiO_2 amorphous catalyst during the reaction could be neglected due to the affinity of SiO_2 for Ni–P alloy particles.

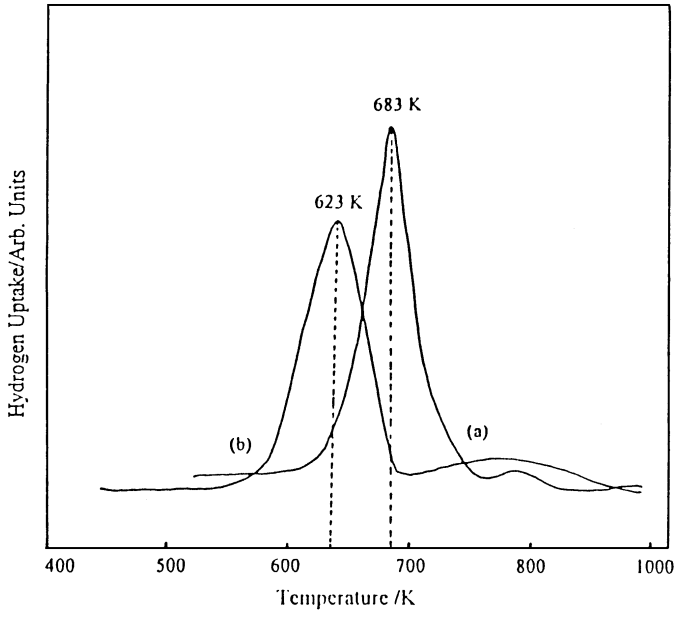

FIG. 9. H_2 TPR curves of (a) $NiCl_2/SiO_2$ sample and (b) the pure $NiCl_2$ sample.

Crystallization Deactivation of Ni–P/SiO_2 Amorphous Catalyst

The following reactions possibly occurred during the catalytic hydrogenation of benzaldehyde (BA) in liquid phase:

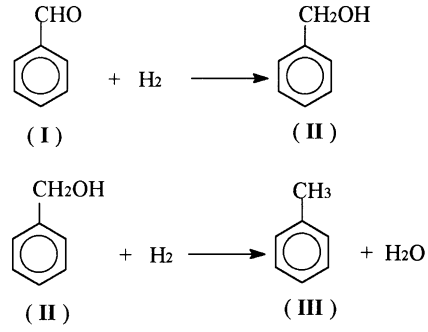

Under the present reaction conditions (pH 4.0), only the toluene (**III**) was identified as the reaction product. Detailed reaction parameters, such as R_{H_2}, the conversion of BA, the TOF value, the general kinetic equation, and the apparent activation energy (Ea), are summarized in Table 4. As the reaction was first-order with respect to P_{H_2} and zero-order with respect to the BA concentration over all the as-employed catalysts, it is reasonable that the TOF value calculated from the BA conversion after reaction for 4 h at 1.0 MPa P_{H_2} also represents the initial rate of reaction since the rate remains constant at constant P_{H_2} when the BA conversion is not very high. On one hand, both the Ni–P/SiO_2 and the Ni/SiO_2 catalysts exhibited a pronounced decrease in the hydrogenation activity after crystallization, possibly due to gathering of Ni particles at high temperature, which resulted in the decrease in the surface active Ni atoms (nearly 50% as shown in Table 1). On the other hand, they also exhibited some different catalytic behaviors. (1) The fresh Ni–P/SiO_2 catalyst exhibited much higher activity than the corresponding Ni/SiO_2 owing to the unique structural characteristics of the Ni–P amorphous alloy (24); (2) the decrease in the activity of the Ni–P/SiO_2 amorphous catalyst was much more rapid than that of the Ni/SiO_2 catalyst; (3) no significant changes in the general kinetic equation, the TOF value, and the Ea were observed after the Ni/SiO_2 catalyst was treated at 873 K, indicating that the decrease in its activity was mainly attributed to the decrease in the surface Ni active atoms. However, a significant crystallization deactivation could be concluded

TABLE 4

Change in the Performance of the As-Prepared Catalysts after Heating Pretreatment[a]

No.	Catalyst	R_{H_2}[b] (mol/h · g Ni)	Kinetic equation	Ea (kJ/mol)	Conv. (%)	TOF[c] (10^{-3}/s)
1	Fresh Ni–P/SiO_2	0.107	$r_1 = k_1 P_{H_2}$	41.7	6.2	2.2
2	Treated Ni–P/SiO_2[d]	0.030	$r_2 = k_2 P_{H_2}$	51.5	1.7	1.0
3	Fresh Ni/SiO_2	0.054	$r_3 = k_3 P_{H_2}$	55.6	3.2	0.88
4	Treated Ni/SiO_2[d]	0.021	$r_4 = k_4 P_{H_2}$	56.4	1.7	0.87

[a] Reaction conditions: 1.0 g catalyst (3.0 wt% Ni), $T = 393$ K, $P_{H_2} = 1.0$ MPa.
[b] Initial rate.
[c] The number of toluene molecules produced per second and per surface Ni atom.
[d] Treated at 873 K for 2.0 h.

since an impressive decrease in the TOF value and a significant increase in the Ea were observed after the crystallization of the Ni–P/SiO_2 amorphous catalyst. This was further confirmed by determining the dependence of the activity on the treating temperature. As shown in Fig. 10. the activity of Ni/SiO_2 catalyst decreased smoothly with the increase of the treating temperature, while, an impressive decrease in the activity of Ni–P/SiO_2 amorphous catalyst was observed in the temperature range from 673 to 873 K, corresponding to the stepwise crystallization of Ni–P/SiO_2 amorphous catalyst. Since the above XPS spectra demonstrated that the electronic interaction between Ni and P or Ni and SiO_2 was not important, such a crystallization deactivation was mainly attributed to the change in the structural properties of the Ni active sites described as follows.

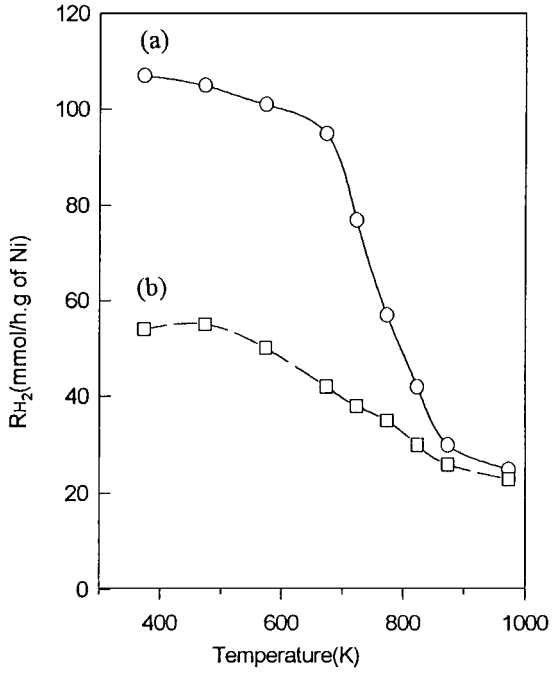

FIG. 10. Dependence of R_{H_2} of (a) Ni–P/SiO_2 amorphous catalyst (○) and (b) Ni/SiO_2 crystalline catalyst (□) on the treating temperature. The Ni loading is 3.0 wt% for each.

(A). The transformation of the Ni–P alloy from the amorphous structure to the crystalline structure. As determined by XRD in Fig. 1, the amorphous Ni–P alloy was homogeneous in its texture with the average composition of $Ni_{86}P_{14}$ while its corresponding crystallized form was relatively heterogeneous, in which the alloy separated into several crystalline species (at least the Ni and the Ni_3P phases). The calculation from the EXAFS spectra (Fig. 3) revealed that the Ni active sites in the Ni–P/SiO_2 amorphous catalyst were more highly unsaturated than those in the corresponding crystallized Ni–P/SiO_2 catalyst. These could account for the higher activity of the Ni–P/SiO_2 amorphous catalyst than that of the crystallized Ni–P/SiO_2 catalyst, since the homogeneous distribution of the highly unsaturated Ni active sites are in favor of the hydrogenation reactions (5, 55, 56).

(B). The change of surface composition. The aforementioned XPS results revealed that the fresh Ni–P/SiO_2 was P-enrich in comparison with the crystallized Ni–P/SiO_2 samples. This could also account for the crystallization deactivation of the Ni–P/SiO_2 amorphous catalyst since the alloying P at low content has been proved to be a promoter on the hydrogenation activity of the Ni-P amorphous catalyst (1, 7, 24).

(C). The change in the strength of hydrogen chemisorption. Since the liquid phase BA hydrogenation reaction is first order with respect to the hydrogen pressure, the strength of hydrogen chemisorption by the Ni–P/SiO_2 amorphous catalyst had an important influence on its hydrogenation activity, especially its TOF value. As shown in Fig. 11, the hydrogen TPD curves revealed that the desorption of the hydrogen from the Ni–P/SiO_2 amorphous catalyst occurred at lower temperature than that from the crystallized Ni–P/SiO_2 catalyst, indicating a stronger absorption bonding between the hydrogen atoms and the active sites in crystallized Ni–P/SiO_2 catalyst. Until now, no quantitative description of the relationship between the TPD results and catalytic behaviors has been reported. According to

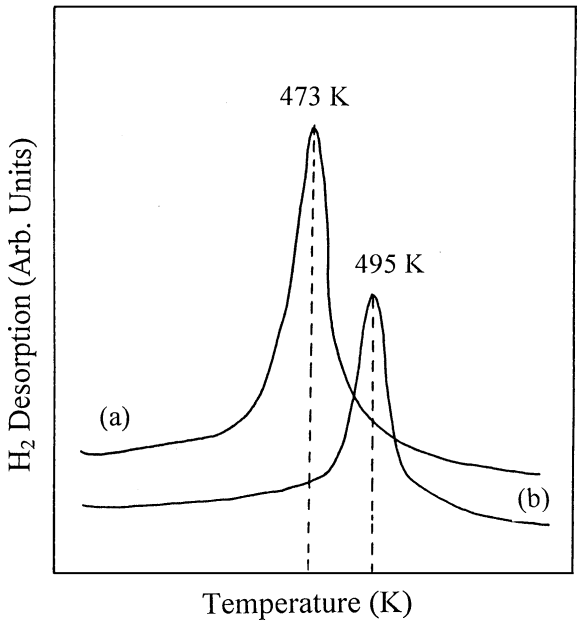

FIG. 11. H_2 TPD curves of (a) the Ni–P/SiO_2 amorphous catalyst (3.0 wt% Ni) and (b) the crystallized Ni–P/SiO_2 catalyst (3.0 wt% Ni).

the well-established catalysis theory, the adsorption bonding for the hydrogen should not be too weak and also not too strong. On one hand, very weak adsorption bonding is unfavorable for the hydrogenation since only very few hydrogen can be adsorbed on the Ni active sites and the dissociation of the hydrogen molecules into hydrogen atoms would be difficult (remember that the BA hydrogenation was first-order with respect to P_{H_2}). On the other hand, very strong adsorption bonding is also unfavorable for the surface hydrogenation reactions since the transfer of the adsorbed dissociated hydrogen atoms to the BA molecules adsorbed on the neighboring Ni active sites would be very difficult, sometimes, nearly impossible. Although the adsorption bonding of Ni–P/SiO_2 amorphous catalyst for hydrogen was weaker than that of the corresponding crystallized Ni–P/SiO_2 catalyst, by comparing the areas of the hydrogen desorption peaks in Fig. 11, it was obvious that the Ni–P/SiO_2 amorphous catalyst adsorbed more hydrogen than the corresponding crystallized Ni–P/SiO_2 catalyst, indicating that the Ni–P/SiO_2 amorphous catalyst had much more surface Ni active sites (as could be seen from the results of the hydrogen chemisorption) and the adsorption bonding strength of Ni–H was not too weak to cause a significant decrease in the amount of the adsorbed hydrogen atoms. Therefore, the fact that Ni–P/SiO_2 amorphous catalyst exhibited higher hydrogenation activity than the crystallized Ni–P/SiO_2 catalyst could also be attributed to its relatively weaker Ni–H bonding, which could facilitate the transfer of the adsorbed hydrogen atoms to the BA molecules adsorbed on the neighboring Ni active sites and, in turn, enhance the surface hydrogenation reactions.

CONCLUSION

The above experimental results revealed that the crystallization process of Ni–P amorphous alloy occurred spontaneously during the pretreatment at high temperature, resulting in the impressive decrease of its catalytic activity during the liquid phase BA hydrogenation. Depositing the Ni–P amorphous alloy on the support could greatly improve its thermal stability and in turn its catalytic properties owing to the stabilizing effect of the support, which were mainly attributed to the high dispersion of Ni–P alloy particles on the support, the affinity of SiO_2 support for the Ni–P alloy particles, and the heat sink of the support. The decrease in the surface active Ni atoms, the decrease in the P content in the surface composition, the transformation from the amorphous structure to the crystalline structure, and the increase in the strength of hydrogen adsorption were the main factors responsible for the decrease in both the hydrogenation activity per gram Ni and the TOF value of the Ni–P/SiO_2 amorphous catalyst during its crystallization process.

ACKNOWLEDGMENTS

This work was supported by the National Natural Science Foundation of China and Shanghai Natural Science Foundation. We are also grateful to SINOPEC and the Committee of Shanghai Education for providing financial support for this study.

REFERENCES

1. Chen, Y., *Catal. Today* **44**, 3 (1998).
2. Deng, J. F., Li, H. X., and Wang, W. J., *Catal. Today* **51**, 113 (1999).
3. Jefimov, J. V., Glasov, M. V., and Vornova, L. I., *Chem. Technol.* **38**, 70 (1986).
4. Molnar, A., Smith, G. V., and Bartok, M., *Adv. Catal.* **36**, 329 (1989).
5. Baiker, A., *Faraday Discuss. Chem. Soc.* **87**, 239 (1989).
6. Ganem, B., and Osby, J. O., *Chem. Rev.* **86**, 763 (1986).
7. Yoshida, S., Yamashita, H., Funabiki, T., and Yonezawa, T., *J. Chem. Soc. Chem. Commun.* 964 (1982).
8. Yamashita, H., Faminade, T., Funabiki, T., and Yoshida, S., *J. Mater. Sci. Lett.* **4**, 1241 (1985).
9. Yu, Z. B., Qiao, M. H., Li, H. X., and Deng, J. F., *Appl. Catal. A: General* **163**, 1 (1997).
10. Li, H. X., Wang, W. J., Zong, B. N., Min, E. Z., and Deng, J. F., *Chem. Lett.* 371 (1998).
11. Li, H. X., Xu, Y. P., and Deng, J. F., *New. J. Chem.* **23**, 1059 (1999).
12. Li, H. X., Wang, W. J., and Deng, J. F., *J. Catal.* **191**, 257 (2000).
13. Coteron, A., and Kenney, C. N., *Appl. Catal. General A* **95**, 237 (1993).
14. Albertos, F., Harji, B. H., Kenney, C. N., and Burstein, G. T., *Appl. Catal.* **65**, 85 (1990).
15. Gasser, A., and Baiker, A., *Appl. Catal.* **48**, 279 (1989).
16. Stancheva, M., Manev, S., Lazarov, D., and Mitov, M., *Appl. Catal. A: General* **135**, 119 (1996).
17. Brown, C. A., and Ahuja, V. K., *J. Org. Chem.* **38**, 2226 (1973).
18. Linderøth, S., and Mørup, S., *J. Appl. Phys.* **69**, 5256 (1991).
19. Linderøth, S., Mørup, S., Koch, C. J. W., Wells, S., Charles, S. W., Wonterghem, J. van, and Meagher, A., *J. Phys. (Paris) Colloq.* **49**, C8 (1991).

20. Linderøth, S., Mørup, S., and Bentzon, M. D., *J. Magn. Magn. Mater.* **83**, 457 (1990).
21. Schreifels, J. A., Maybury, P. C., and Swartz, W. E., Jr., *J. Org. Chem.* **46**, 1263 (1980).
22. Dragieva, I., Rusev, Kr., and Stanimirova, M., *J. Less-Common Met.* **158**, 295 (1990).
23. Yamashita, H., Yoshikawa, M., Funabiki, T., and Yoshida, S., *J. Chem. Soc. Faraday Trans I* **82**, 1771 (1986).
24. Yamashita, H., Yoshikawa, M., Funabiki, T., and Yoshida, S., *J. Catal.* **99**, 375 (1986).
25. Li, H. X., Chen, H. Y., Dong, S. Z., Yang, J. S., and Deng, J. F., *Appl. Surf. Sci.* **125**, 115 (1998).
26. Yang, J. S., Li, H. X., and Deng, J. F., *Appl. Surf. Sci.* **147**, 33 (1999).
27. Liu, B. S., Li, H. X., and Deng, J. F., *J. Membr. Sci.* **135**, 33 (1997).
28. Deng, J. F., and Zhang, X., *Appl. Catal.* **37**, 339 (1988).
29. Li, H. X., Dai, W. L., Shen, C., and Deng, J. F., *Chem. Lett.* 133 (1997).
30. Xie, S. H., Qiao, M. H., Li, H. X., and Deng, J. F., *Appl. Catal. A: General* **176**, 129 (1999).
31. Wang, W. J., Qiao, M. H., Li, H. X., and Deng, J. F., *Appl. Catal. A: General* **168**, 151 (1998).
32. Wang, W. J., Qiao, M. H., Li, H. X., and Deng, J. F., *Appl. Catal. A: General* **166**, L243 (1998).
33. Wang, W. J., Qiao, M. H., Li, H. X., and Deng, J. F., *J. Chem. Technol. Biotechnol.* **72**, 280 (1998).
34. Chen, Y. Z., and Ling, K. S., *J. Theor. Chinese I. Ch. E.* **22**, 103 (1991).
35. Gil, A., *Appl. Catal. General A* **109**, 167 (1994).
36. Bartholomew, C. W., and Farrauto, R. J., *J. Catal.* **45**, 41 (1976).
37. Zhang, X. P., and Deng, J. F., *Chinese J. Catal.* **11**, 173 (1990).
38. Palmer, M. B., Jr., and Vannice, M. A., *J. Chem. Technol. Biotechnol.* **30**, 205 (1980).
39. Chen, J., Lu, G., and Ma, L., *Fudan Univ. Acta.* **28**, 78 (1989).
40. Huchital, D. A., and McKeon, R. T., *Appl. Phys. Lett.* **20**, 158 (1972).
41. Yokoyama, A., Komiyama, H., Inoue, H., Masumoto, T., and Kimura, H. M., *J. Catal.* **68**, 355 (1981).
42. Zhang, H., Lu, B., Luao, X., Sheng, X., and Yu, Z., *Acta Chim. Sinica* **44**, 133 (1986).
43. Schwarz, J. A., Contescu, C., and Contescu, A., *Chem. Rev.* **95**, 477 (1995).
44. Li, H., Li, H. X., and Deng, J. F., *Appl. Surf. Sci.* **152**, 25 (1999).
45. Yoshida, S., Yamashita, H., and Funabiki, T., *J. Chem. Soc., Faraday Trans. I* **80**, 1435 (1984).
46. Yamashita, H., Yoshikawa, M., Funabiki, T., and Yoshida, S., *J. Chem. Soc., Faraday Trans. I* **81**, 2485 (1985).
47. Okamoto, Y., Nitta, Y., Imanaka, T., and Teranishi, S., *J. Chem. Soc., Faraday Trans. I* **75**, 2027 (1979).
48. Beilin, B., Traverse, A., Szasz, A., and Machizaud, F., *J. Phys. F: Met. Phys.* **17**, 1913 (1987).
49. O'Handley, R. C., Hasegawa, R., Ray, R., and Chou, P., *Appl. Phys. Lett.* **29**, 330 (1976).
50. Ivkov, J., and Babic, E., *J. Phys. F: Met. Phys.* **15**, L161 (1985).
51. Krasser, W., Fadini, A., and Renouprez, A. J., *J. Catal.* **62**, 94 (1980).
52. Campelo, J. M., Garcia, A., Gutierrez, J., Luna, M., D., and Marinas, J. M., *Appl. Catal.* **7**, 307 (1983).
53. Bartherlomew, C. H., and Uken, A. H., *Appl. Catal.* **7**, 169 (1983).
54. Zhang, L., Lin, J., and Chen, Y., *J. Chem. Soc. Faraday Trans. I* **88**, 497 (1992).
55. Ghuge, K. D., Bhat, A. N., and Babu, G. P., *Appl. Catal. General A* **103**, 183 (1993).
56. Deng, J. F., Yang, J., Sheng, S., and Chen, H., *J. Catal.* **150**, 434 (1994).